A Review of Lithium Niobate Modulators for Fiber-Optic Communications Systems

Ed L. Wooten, *Member, IEEE*, Karl M. Kissa, *Member, IEEE*, Alfredo Yi-Yan, Edmond J. Murphy, *Senior Member, IEEE*, Donald A. Lafaw, Peter F. Hallemeier, *Member, IEEE*, David Maack, *Member, IEEE*, Daniel V. Attanasio, Daniel J. Fritz, Gregory J. McBrien, *Member, IEEE*, and Donald E. Bossi, *Member, IEEE*

Invited Paper

***Abstract*—The current status of lithium-niobate external-modulator technology is reviewed with emphasis on design, fabrication, system requirements, performance, and reliability. The technology meets the performance and reliability requirements of current 2.5-, 10-, and 40-Gb/s digital communication systems, as well as CATV analog systems. The current trend in device topology is toward higher data rates and increased levels of integration. In particular, multiple high-speed modulation functions, such as 10-Gb/s return-to-zero pulse generation plus data modulation, have been achieved in a single device.**

***Index Terms*—Electrooptical modulators, lithium niobate, optical modulator, waveguide devices.**

I. Introduction

OVER THE past decade, as the demand for telecommunications services and bandwidth has boomed, the need for and advantages of external modulation in fiber-optic transmission systems has been firmly established. In higher speed digital communication applications, fiber dispersion has limited system performance. Lithium niobate ($LiNbO_3$) external modulators provide both the required bandwidth and the equally important means for minimizing the effects of dispersion. Unlike direct modulation of a laser diode, $LiNbO_3$ guided-wave modulators can be designed for zero-chirp or adjustable-chirp operation. Zero-chirp and negative-chirp modulators help to minimize the system degradation associated with fiber dispersion. In analog systems, linearized external modulators can provide very low modulation distortion.

Advances in $LiNbO_3$ modulator device technology have enabled stable operation over temperature, very low bias-voltage drift rates, and bias-free devices. These advances in device and material technology have been accompanied by significant investments in guided-wave device manufacturing. The net result today is a strong demand for and an ample supply of high-quality $LiNbO_3$ modulator components for use in fiber-optic communication systems. In this paper, we will provide an overview of the present state of $LiNbO_3$ modulator technology. More detailed and complementary information can be found in recent publications, which cover devices and system applications [1], switching technology [2], and guided-wave devices in general [3].

Section II of this paper describes the basic techniques used to fabricate $LiNbO_3$ guided-wave devices. Section III discusses various modulator device designs, structures, and functions. Section IV describes the performance of $LiNbO_3$ devices in digital systems. Section V covers some nondigital applications for $LiNbO_3$ modulators. Section VI discusses the product development cycle and manufacturability of these devices. Section VII reviews reliability data available from the field and accelerated-aging tests.

Manuscript received September 17, 1999.
The authors are with JDS Uniphase Corp., Bloomfield, CT 06002 USA.
Publisher Item Identifier S 1077-260X(00)01136-9.

II. Device Fabrication

Lithium niobate has a very high intrinsic modulation bandwidth, but device switching speeds are limited by a variety of physical constraints. Modulation is produced by a voltage-induced change in the refractive index. The achievable index change is small and, thus, either large voltages or long electrode lengths are needed to obtain sufficient modulation. A useful figure of merit for modulation is the product of the switching voltage and the electrode length. For lengths that allow reasonable voltages, the capacitance of lumped element electrodes would limit the bandwidth to less than 1 GHz. By using travelling wave electrodes, in which the electrical signal propagates along the same direction as the optical wave, much higher bandwidths can be obtained. In this case bandwidths are limited by the mismatch between the electrical and optical propagation constants as well as by the electrical attenuation of the electrode [4]. Theoretical and experimental work has led to electrode structures optimized for 10-Gb/s digital modulation [5].

Fig. 1 depicts a cross-sectional view of an x-cut $LiNbO_3$ Mach–Zehnder interferometer (MZI) modulator, where the critical dimensions of the modulator structure are shown. Wave velocity is a function of the material properties and the waveguide cross-sectional dimensions. Because the modulator can be several centimeters long, preservation of cross-sectional dimensions along the length of a device presents a challenge not only from the standpoint of fabrication but also in the

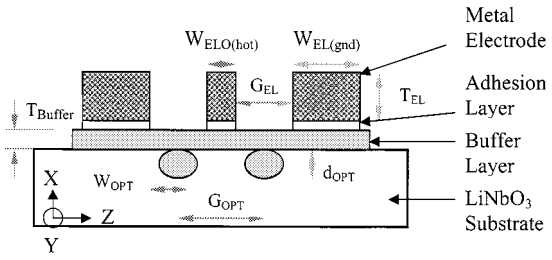

Fig. 1. Cross-sectional view of an x-cut modulator with coplanar-waveguide (CPW) radio-frequency electrodes.

choice and compatibility of materials used. Required materials include the electrooptic substrate, electrode metal, electrode adhesion layer, buffer layer, and the dopant used for fabrication of the optical waveguides.

A. $LiNbO_3$ Wafers

$LiNbO_3$ has been the material of choice for the fabrication of electrooptic modulators due to its combination of high electrooptic coefficients and high optical transparency in the near infrared wavelengths used for telecommunications. Its high Curie temperature (1100 °C–1180 °C) makes it practical for fabrication of low-loss optical waveguides through indiffusion of metals [6]. $LiNbO_3$ is also thermally, chemically, and mechanically stable and is compatible with conventional integrated-circuit processing technology.

Wafers with high optical homogeneity and surface flatness are needed in the fabrication of integrated optical devices. $LiNbO_3$ wafers are obtained from boules grown using the Czochralski technique. During the growth process, care is taken to ensure that Fe ion contaminants are eliminated, or kept to a minimum, in order to reduce the susceptibility of the crystal to photorefractive optical damage. $LiNbO_3$ is particularly susceptible to optical damage at wavelengths below 1 μm. However, for wavelengths greater than 1 μm, photorefractive damage is generally negligible for optical powers less than 100 mW.

$LiNbO_3$ wafers with diameters up to 100 mm are commercially available in different crystal cuts (x-, y-, and z-cut) with the choice of cut depending upon the application. The handling of x- and y-cut wafers during the fabrication process is fairly straightforward, whereas z-cut wafers require special handling procedures because the crystal's piezoelectric and pyroelectric properties produce electrical charge accumulation on the z-faces during processing. Modulators made on z-cut wafers also require special design and packaging to minimize bias drift due to charge migration and the buildup of pyroelectric charges.

B. Waveguide Fabrication

$LiNbO_3$ waveguides have been traditionally fabricated by indiffusion of Ti at temperatures near 1000 °C. The process is straightforward, but precautions must be taken to suppress the out-diffusion of Li from the surface of the substrate. A Li-deficient surface results in an unwanted planar waveguide for z-polarized light and can seriously affect modulator performance. The presence of Ti in the crystal increases both the ordinary and the extraordinary indexes of refraction. Hence, for suitable doping concentrations, both TE and TM modes will propagate along the waveguides.

An alternative method for fabricating $LiNbO_3$ waveguides is through the annealed proton exchange (APE) process [7]. Proton exchange [8] is a low-temperature process (~120 °C–250 °C) whereby Li ions from the $LiNbO_3$ wafer are exchanged with protons from an acid bath. Proton exchange can only be applied to x- and z-cut wafers; the acid chemically etches y-cut wafers. Exchanged layers exhibit an increase in the extraordinary index; the ordinary index is left virtually undisturbed or even reduced. APE waveguides are, consequently, polarizing waveguides. The proton exchange is followed by a high-temperature anneal. The annealing step in the APE process is crucial in obtaining high-quality electrooptic waveguides. The annealing process successfully addresses the problems of index instability [9], [10] and deterioration of the electrooptic effect [11] exhibited by proton-exchanged waveguides without anneal. Accelerated aging studies carried out on x-cut APE directional couplers and Mach–Zehnder modulators have shown no degradation of device performance over a 13-year lifetime at 125 °C and a 25-year lifetime at 95 °C [12], [13].

Preservation of waveguide cross-sectional properties across the wafer requires good uniformity in Ti film deposition as well as uniformly flat thermal zones in furnaces used for the diffusion or exchange/anneal processes. Careful screening of wafers for surface flatness is key to minimizing waveguide-width variation across the wafer during mask definition by photolithography. Last, process parameters such as Ti film thickness, diffusion temperature, and time can be tailored to yield high-quality stripe waveguides, which exhibit low propagation loss, optimum field confinement, and good waveguide-to-fiber coupling.

Almost all commercially available 2.5- and 10-Gb/s $LiNbO_3$ modulators use stripe optical waveguides. As modulation speeds increase to greater than 20 Gb/s, ridge waveguides on z-cut substrates will be required to achieve lower drive voltages and reduce device lengths [14]. A ridge waveguide under the active (or "hot") electrode concentrates the flux of the applied electric field within the waveguide and provides tighter confinement of the optical mode. Both effects increase the overlap between the applied electric field and the optical mode in a z-cut arrangement, thus providing a lower switching voltage. $LiNbO_3$ ridges a few micrometers deep can be obtained by wet etching [15], [16] or ion-milling [17] techniques. Smooth ridge sidewalls as well as good control of etch depth and sidewall direction are key in achieving low-loss waveguides with good mode confinement.

C. Electrode Fabrication

RF electrodes are fabricated either directly on the surface of the $LiNbO_3$ wafer or on an optically transparent buffer layer to reduce optical loss due to metal loading and provide a means for optical/RF velocity matching. In general an adhesion layer, such as Ti, is first vacuum deposited on the wafer, followed by the deposition of a base layer of the metal in which the electrodes are to be made. The electrode pattern is then photolithographically defined. High-speed modulators incorporate RF electrodes whose thickness can range from a few micrometers to greater than 15 μm. Special lithographic processes are needed to define

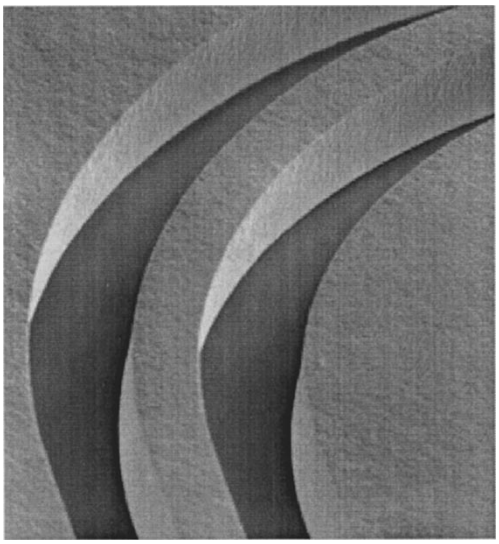

Fig. 2. SEM picture of 18-μm-thick gold-plated CPW electrodes at a region where the electrodes are making a bend.

the thick mask and to ensure that the electroplating process preserves the cross-section of the RF electrode along the length of the device.

Gold is generally used as the electrode metal. Plating processes yielding high-purity metal, small grain size, minimum feature distortion, and reasonable plating rate are key to obtaining good RF performance. Various plating chemistries, dry or in solution, are commercially available. Each chemistry works best in conjunction with a particular continuous and/or pulsed current supply as well as a particular mask material. After plating, the mask is removed and the metal in the gaps is etched away. Fig. 2 shows a scanning electron microscope (SEM) picture of a typical gold-plated coplanar-waveguide electrode fabricated for a 10-Gb/s digital modulator.

D. Dicing and Polishing

In contrast to semiconductor materials such as GaAs or InP, $LiNbO_3$ substrates do not cleave readily. Substrates containing an array of finished modulators are cut from the $LiNbO_3$ wafer using conventional water-cooled diamond saws. The substrate end faces are cut at an angle to the waveguides in order to eliminate reflections and are then polished to an optical finish. A good optical finish and a sharp edge are required at both the input and output optical facets of the device to ensure good fiber-to-waveguide coupling. For ease of handling, the modulators on a substrate are individually tested before the substrate is diced into individual components.

Cleanliness must be maintained throughout the modulator fabrication process. Debris from dicing and particulates from polishing compounds are contaminants that can negatively impact the performance and long-term reliability of the modulators, and must therefore be removed during chip cleaning operations.

E. Pigtailing, Packaging, and Test

To utilize $LiNbO_3$ modulators in real-world applications, the integrated-optic chip must be pigtailed and packaged in order that optical and electrical signals can be efficiently and effectively directed into and away from the device. Three principle subassemblies or subcomponents are used in the manufacture of packaged $LiNbO_3$ modulators. The three subassemblies are, namely, the integrated-optic chip, optical-fiber assemblies, and electrical or RF interconnects and housing. The fabrication of the integrated-optic chip was described in detail in the preceding paragraphs of this article.

$LiNbO_3$ modulators can be packaged in either hermetic or nonhermetic housings, depending upon the application, operating environment, and methods and materials utilized in the modulator manufacturing process. Reference [18] provides a comprehensive description of the packaging techniques used to produce hermetically packaged $LiNbO_3$ modulators. For devices designed to operate within telecommunication central-office environments, nonhermetic packaging has proven both sufficient and cost effective for meeting the necessary reliability and qualification requirements [19].

Due to the polarization dependence of the electrooptic effect, the polarization state of the input light supplied to the modulator must be carefully controlled and maintained to achieve optimum performance. Hence, most $LiNbO_3$ modulators utilize polarization-maintaining fiber for the input pigtail, while the output fiber is typically standard single-mode fiber. During the preparation of the input and output optical fiber subassemblies, a small tube or block is attached to the end of each fiber. This tube is angle cut and polished to minimize back-reflections from the fiber-to-$LiNbO_3$ interface. The tube also increases the surface area and bond strength of the pigtail joint, thereby ensuring long-term stability and reliability. Ultraviolet-curing or thermal adhesives are used to attach the fiber subassemblies to the $LiNbO_3$ chip. The fiber subassemblies are typically designed with a strain-absorbing bow to accommodate the differential thermal expansion among the $LiNbO_3$ chip, the fiber, and the metallic housing [18].

Electrical interconnects are attached and soldered to the modulator housing, thereby creating the third subassembly. The pigtailed $LiNbO_3$ chip is attached to the package using a compliant adhesive that mechanically decouples the optical assembly from the package and absorbs thermally induced strains [20]. Last, electrical interconnection between the package and the $LiNbO_3$ chip is accomplished using either wire or ribbon bonds. For high-frequency operation, the dimensions of the bond must be carefully controlled to achieve optimal performance.

Once all three subassemblies are copackaged, the modulator must be sealed and tested as a completed, functional unit. Key parameters that are typically measured during final test include: optical loss, switching voltage, optical on/off extinction, bias stability, and microwave/RF properties such as S_{11} and S_{21}. Oftentimes, some of these performance parameters are measured over the operating temperature range of the device. Bit-error-rate and eye-diagram measurements are not typically required on each production device. These measurements are often performed during the design verification and validation stages of product development, and only the aforementioned parameters need to be measured in production.

III. Device Design

The basic building blocks for lithium niobate modulators and switches generally fall into one of two categories: MZI type or

directional coupler type [21]. In the MZI, light is split into two optical paths that are isolated from one another. The applied electric field from an electrode modifies the relative velocities of the two beams via the electrooptic effect, resulting in variable interference when the two paths are recombined at the output. In the directional coupler approach, light is injected into two modes of a waveguide structure. The applied field modifies the relative velocities of the two modes as well as the coupling between the modes. The two most common examples of the directional coupler type are the reversed delta-β coupler [22] and the digital optical switch [23]–[27]. The reversed delta-β coupler is compact and can be tuned with modest voltages (10–20 V). The digital optical switch requires higher drive voltages (40–50 V) but can be constructed as a polarization-independent switch. The MZI works well with high-bandwidth electrode structures requiring tens of micrometers of spacing between waveguides, and long electrodes are needed to reduce drive voltages ($\leq$6 V). The directional-coupler-type switches are typically used for lower speed switching applications where small size and polarization diversity may be required, and tight electrode gaps (<10 μm) are more easily accommodated.

The first choice encountered in designing a $LiNbO_3$ modulator is the orientation of the crystal axes to the waveguides and electrodes. The crystal cut affects both modulator efficiency, as denoted by half-wave voltage V_π, and modulator chirp, which is described by the chirp parameter α. The difference is apparent in Fig. 3, which shows the four most common electrode structures used in MZI-type switches. The strongest component of the applied electric field must be aligned with the z-axis of the crystal, which has the highest electrooptic coefficient. This requires that the waveguide be placed between the electrodes for an x-cut configuration and beneath the electrodes for z-cut. Because the electrodes are placed on top of the waveguides, z-cut devices always require a buffer layer to minimize attenuation of the optical mode due to metal absorption. Z-cut devices also typically employ conductive buffer layers and charge bleed layers to mitigate dc drift and pyroelectric charge buildup, respectively [18]. X-cut devices do not inherently need a buffer layer because the electrodes are not placed directly above the waveguides; however, to achieve multigigahertz operation, broad-band x-cut devices do use a buffer layer for velocity matching of the RF and optical waves.

The applied electric field and electrooptic efficiency of various electrode topologies can be modeled using quasi-static techniques such as finite-element or finite-difference methods [28]. These techniques also provide the microwave properties of the electrode (velocity, impedance, and loss). RF loss can also be adequately determined at high frequencies (>2 GHz) with Wheeler's inductance rule [29]. In general, thick electro-plated electrodes ($\geq$15 μm) have low RF loss ($\leq$0.5 dB·cm^{-1}·GHz$^{-0.5}$) and enhanced velocity matching due to the presence of electric flux in the air gap between electrodes. Buffer layers are required for broad-band velocity matching on both x- and z-cut devices due to the high RF dielectric constants of lithium niobate ($\varepsilon_{x,z} = 44, 28$) relative to the optical dielectric constants ($\varepsilon_{x,z} = 4.6, 4.9$).

X-cut electrode topologies [Fig. 3(a) and (b)] result in chirp-free modulation due to the push–pull symmetry of the

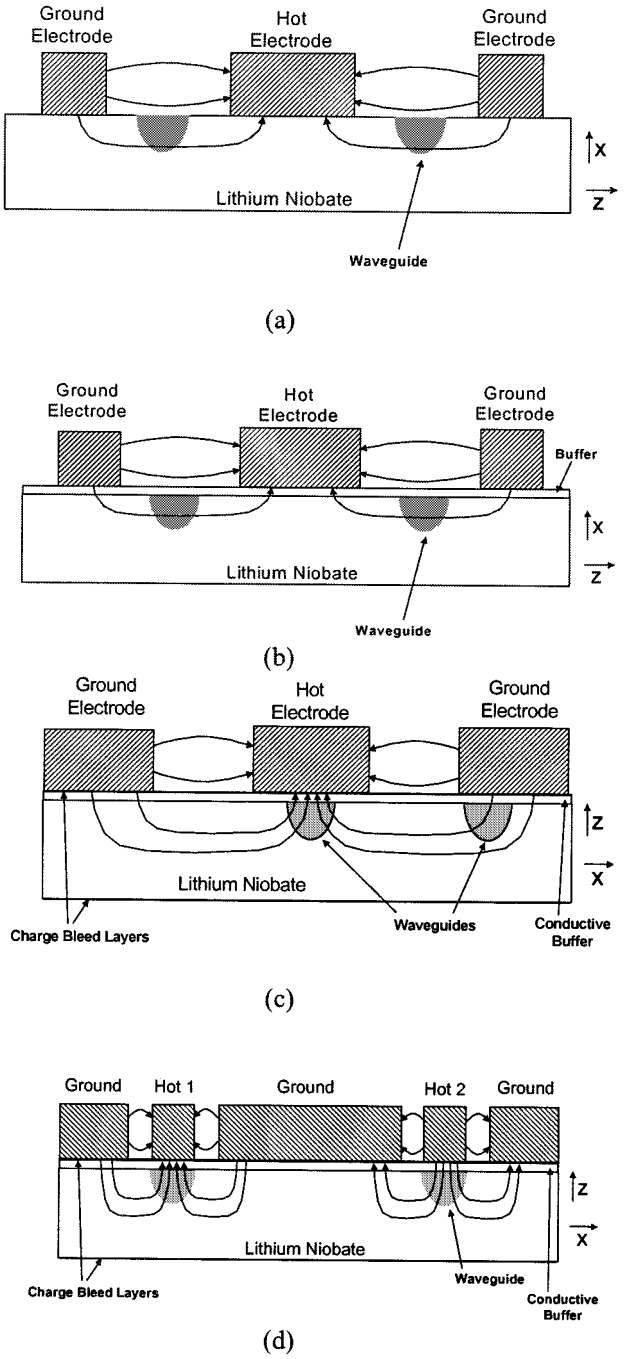

Fig. 3. Most common electrode configurations for (a) nonbuffered x-cut, (b) buffered x-cut, (c) buffered single-drive z-cut, and (d) buffered dual drive z-cut.

applied fields in the electrode gaps. In z-cut devices, the waveguide positioned underneath the hot electrode experiences an RF field flux that is more concentrated, resulting in a factor of two improvement in overlap between RF and optical field, relative to x-cut. However, the overlap under the z-cut ground electrode is reduced by a factor of three, relative to x-cut; therefore, the overall improvement in z-cutV_π (relative to the x-cut V_π) is only about 20% for single-drive modulators. The difference in overlap between the two z-cut waveguides results in a chirp parameter of approximately –0.7.

By employing a dual-drive topology, in which the push–pull effect is produced by the driver circuit, the factor of two im-

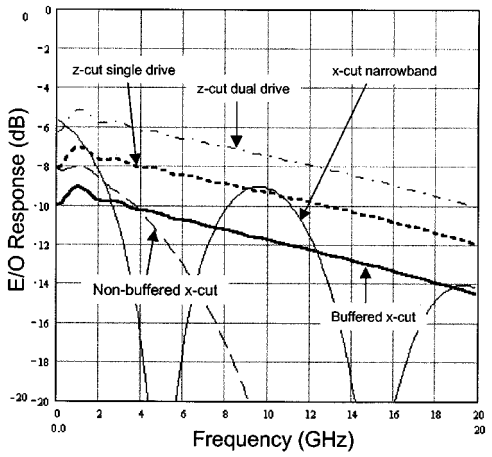

Fig. 4. Calculated electrooptic response for several devices designed for broad-band digital or RZ pulsing applications at 2.5 or 10 Gb/s using conventional electrode and waveguide structures (no ridges or Δn enhancement). Electrode lengths were chosen to be representative of devices used in actual applications and are shown in Table I.

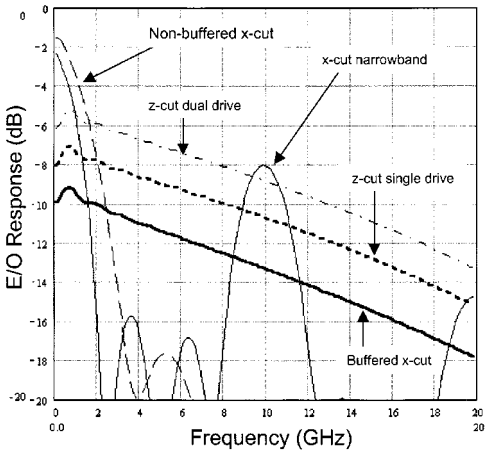

Fig. 5. Calculated electrooptic response for the case where all modulators have a 5-cm electrode length (conventional electrode and waveguide structures, no ridges or Δn enhancement).

provement in overlap under the hot electrode can be utilized in both arms of the MZI at the expense of increased RF circuit complexity. Balancing the two drive levels results in zero-chirp operation. Imbalancing the two drive levels provides electronically programmable chirp.

Nonbuffered x-cut is the overall winner in electrooptic efficiency per unit length, having about a 30% lower $V_\pi L$ than the z-cut waveguide beneath the hot electrode. Unfortunately, velocity mismatch of nonbuffered x-cut limits bandwidth, and the 25-Ω electrode impedance introduces additional penalties due to impedance mismatch and RF loss. RF electrodes on buffered x- and z-cut substrates can be designed for velocity matching and impedances near 40 Ω.

A number of methods have been employed to enhance the electrooptic efficiency. Ridge waveguides further enhance the focusing of electric flux under the hot electrode and have been used to demonstrate V_π of 3.5 and 5.1 V for z-cut modulators with 30- and 70-GHz bandwidths (3 dB electrical), respectively [28]. A 15% reduction of V_π has also been demonstrated by using ridge structures in an x-cut device without a buffer layer and by using lumped-element (low-frequency) electrodes [30]. The overlap between the applied electric field and the optical fields can also be improved in both x- and z-cut by increasing the waveguide refractive index and narrowing the ground electrode width [31].

The electrooptic efficiency at modulation frequency can be improved at the expense of bandwidth by using RF phase-matching techniques such as phase reversal or intermittent-interaction electrodes [32]. These narrow-band techniques allow the buffer/electrode structure to be optimized for the best field overlap, while RF phase-matching is achieved by flipping the polarity of the electrooptic interaction periodically, or by moving the electrode away from the waveguide when the walk-off between RF and optical fields exceeds 180°. More complex electrode structures allow further improvement in phase-matching while still maintaining the high level of field overlap, resulting in approximately 40% improvement in modulation efficiency compared to phase reversal [33].

TABLE I
NORMALIZED ELECTRODE LENGTHS USED IN CALCULATION SHOWN IN Fig. 4

Electrode / crystal cut	Application	Electrode Length
Non-buffered x-cut	2.5 Gb digital	1.0
Buffered x-cut	10 Gb digital	2.2
x-cut narrowband	10 Gb RZ pulse	1.5
z-cut single drive	10 Gb digital	2.2
z-cut dual drive	10 Gb digital	2.2

Narrow-band devices are well suited for return-to-zero (RZ) pulsing applications because the pulse generator is typically driven with a sinusoidal signal at the clock frequency [34].

The electrooptic efficiency versus modulation frequency is compared in Figs. 4 and 5 for the various electrode geometries and crystal cuts of Fig. 3. A narrow-band x-cut modulator for RZ pulsing is included as well [33]. The response curves represent electrical power at the receiver's photodetector per unit of total electrical power into the modulator (add the power into both ports for dual drive). Conventional electrode and waveguide structures are assumed [28], [35], that is, CPW electrodes are assumed and no ridges or Δn enhancement are utilized. RF properties and RF-optical overlap have been calculated using finite difference quasi-static field analysis. Optical mode profiles typical of conventional single-mode stripe wave-guides are used in the RF-optical field overlap calculation. The electrode properties and dc electrooptic efficiency are inserted into an electrooptic response model that accounts for reflections from the RF termination [35].

Fig. 4 shows the calculated electrooptic response for several devices designed for broad-band digital or RZ pulsing transmission applications at 2.5 or 10 Gb/s using conventional electrode and waveguide structures (no ridges or Δn enhancement). The electrode lengths were chosen to be representative of devices used in actual applications and are shown in Table I, normalized to the shortest electrode (nonbuffered x-cut). The application for which each device would be best suited is also listed in Table I. Fig. 5 shows the electrooptic response for the case where all modulators have a 5-cm electrode length. Note that

the plots in Figs. 4 and 5 are of the same format as an S_{21} (electrooptic electrical dB) network analyzer measurement. RF loss from packaging is neglected in the plots of Figs. 4 and 5, in order that raw electrooptic performance can be compared.

The comparison of electrooptic efficiency in Fig. 4 reveals some interesting results. As expected, z-cut dual drive is the most efficient, given its long length, velocity matching, and high overlap efficiency. The 4-dB advantage over buffered x-cut is mainly due to the factor-of-two improvement in RF-optical overlap minus the 3-dB penalty for two inputs. Single-drive z-cut only boasts a 2-dB advantage over buffered x-cut, and is surpassed slightly at 10 GHz by narrow-band x-cut, which is 30% shorter. Nonbuffered x-cut begins near the efficiency of z-cut single drive, but rolls off faster due to RF-optical velocity mismatch. Note that the improved performance of z-cut dual-drive device comes at the expense of greater sophistication in delivery of RF drive signals to the modulator, a complication that is an issue at 10 Gb/s and becomes problematic at higher bit rates such as 40 Gb/s.

The electrooptic efficiency for the case where all electrodes are 5 cm is shown in Fig. 5. The narrow-band x- cut device is the overall winner at 10 GHz, even surpassing the z-cut dual-drive structure by about 1 dB. The low RF electrode loss and high overlap efficiency of the narrow-band electrodes on nonbuffered x-cut substrates account for the improved performance. In the narrow-band design, the RF loss can be minimized with little constraint from velocity or impedance-matching concerns, a degree of freedom that becomes significant for longer electrode lengths.

One other factor that affects modulator design is bias voltage drift. For MZI type modulators, the optical output power versus drive voltage transfer function is sinusoidal, with the ideal bias point near the half power point (quadrature). Quality of transmitted digital data can suffer if the bias point shifts too much over time, generally requiring an active feedback circuit to monitor and adjust the bias voltage. Alternatively, the bias point can be preset in manufacturing, eliminating the need for a feedback circuit, or at the very least reducing the level of applied dc voltage. The long-term dc drift behavior is best described by an RC ladder model [36]. The initial applied field is determined by capacitive voltage division through the ladder. The long-term field is determined by resistive voltage division. The resistors and capacitors in the model are set by process parameters and conditions used to fabricate the waveguides and electrodes. Accelerated aging tests reveal that bias voltage for a device using Ti indiffused waveguides will not change by more than a factor of two from the initial bias voltage, over a 20-year lifetime at typical operating temperatures.

Lithium niobate modulator technology easily accommodates integration of multiple functions. The level of integration is mainly limited by the size of the wafer and the length of the different building blocks. A simple example of integration is a series cascade of a low-speed MZI and a high-speed MZI to form a variable optical attenuator plus data modulator. The efficiency per unit length of the narrow-band x-cut electrode permits an RZ pulse generator to be integrated in series with a broad-band data modulator [33]. Alternatively, an MZI and phase modulator can be integrated, both having narrow-band electrode structures, to form a chirped RZ pulse generator [33] needed for long-distance transmission [34], [37]. Integration of MZI's in series or parallel has been proposed and demonstrated for linearization of the transfer function for cable TV and other analog transmission applications [38]–[40]. Last, hybrid integration of photodetectors with the lithium niobate chip is readily accomplished for power monitoring functions.

IV. Systems Requirements and Digital Performance

In recent years, $LiNbO_3$ devices have successfully addressed the modulation requirements in digital fiber-optic time-domain-multiplexed (TDM) and wavelength-division-multiplexed (WDM) systems. Modulators have become a critical component in the majority of today's long-haul-terrestrial and submarine optical networks. The appropriate modulator architecture is chosen for a given system implementation based on performance criteria and transmission format.

When designing and characterizing a fiber-optic transmission system, a baseline measurement of the transmitted signal is made at the modulator output through analysis of the signal's time-domain properties. This modulated optical signal is then launched into the fiber-optic link. Signal degradation, resulting from numerous fiber processes, amplifier noise, and other link components, is quantified by measuring the detected signal. A measurement of the bit error rate (BER) determines the accuracy with which the optical receiver is able to differentiate between digital "one" and "zero" bits. This fundamental challenge of maintaining signal quality through the optical fiber link determines the performance requirements of the modulator.

The predominant technique used for telecommunications transmission in optical fiber has been on–off keying (OOK), or intensity modulation with direct detection, where the optical intensity is gated in a shuttering fashion. Data encoding has predominantly utilized a nonreturn-to-zero (NRZ) format, where an arbitrary data stream of "one" and "zero" symbols is directly encoded as high and low optical powers, respectively. Advantages of OOK include minimizing the fiber link degradation due to group velocity dispersion, because NRZ data coding provides a narrow-spectrum signal, and ease of data recovery at the receiver. OOK is adequate for links operating at data rates of 2.5 Gb/s for spans up to 1000 km and 10 Gb/s for spans up to 500 km, utilizing traditional and nonzero-dispersion-shifted single-mode fibers.

A typical NRZ transmitter incorporating a $LiNbO_3$ modulator is shown in Fig. 6. Digital OOK waveforms are typically presented in the form of an "eye" diagram, which is the superposition of all "one" and "zero" states of a pseudorandom bit sequences (PRBS) within one bit window. Fig. 7(a) and (b) shows $LiNbO_3$ externally modulated eyes at 2.5 and 10 Gb/s, respectively.

The center of the eye is required to receive no light intensity, or "hits," since the receiver decision circuitry operates in this region using a preset intensity threshold. A larger "no-hit" zone improves the accuracy of the receiver and lowers the BER. Since the processes that degrade the eye are typically stochastic in nature, long sampling times of the transmitted signals are required to accurately quantify the system's BER. Transmitter metrics,

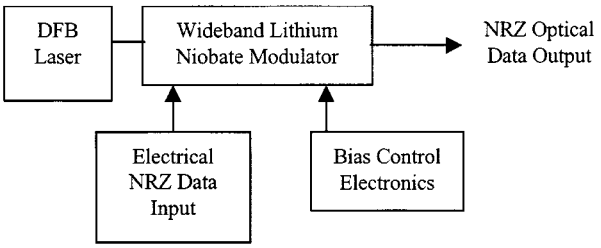

Fig. 6. Data modulator topology for NRZ transmission.

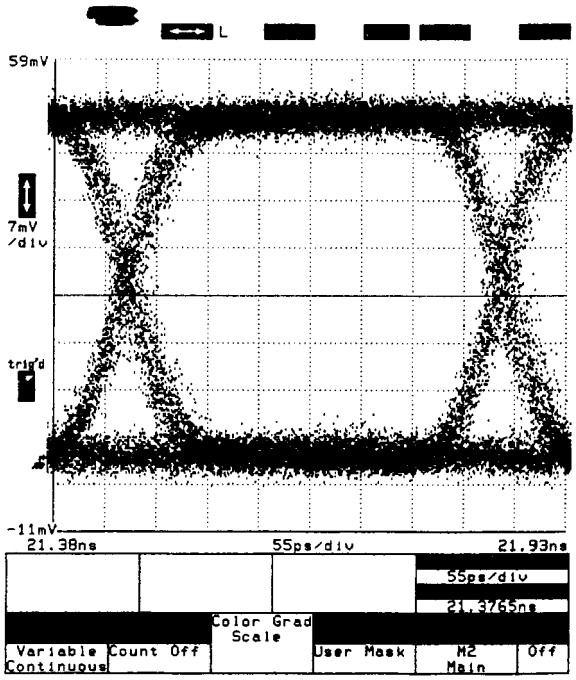

(a)

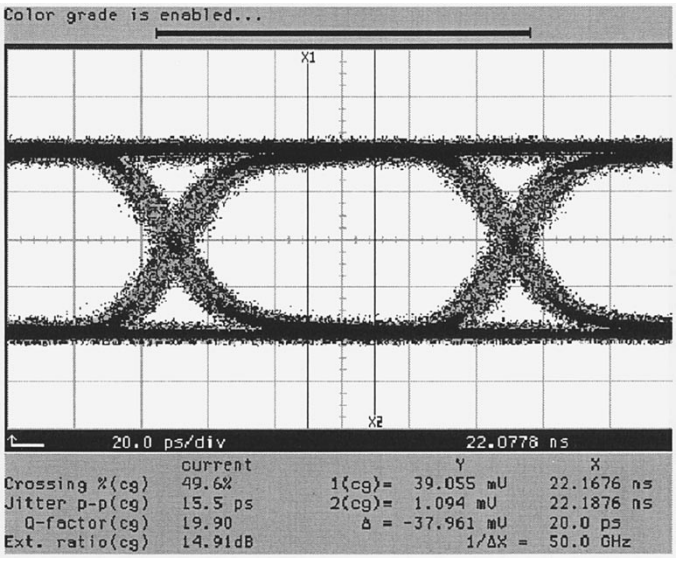

(b)

Fig. 7. $LiNbO_3$ externally modulated eyes at (a) 2.5 and (b) 10 Gb/s.

including average launch power, optical extinction ratio, transition rise and fall times, timing jitter, transition crossing percentage, and Q parameter, have been developed to quantify the quality of the digital signal. The key performance parameters of the modulator that impact these metrics, and therefore determine system performance, are switching voltage, S_{21} electrical-to-optical response, S_{11} electrical return loss, optical extinction ratio, excess optical loss, and optical chirp of the modulated signal.

The S_{21} parameter relates the modulator's high-frequency switching voltage to the electrooptic efficiency of the device at low frequency, usually denoted as V_π at dc. Practical implementations of digital systems can tolerate up to 3-dB rolloff in efficiency at the highest frequency in the modulated signal's spectrum. In digital systems, the requirement for wide-band operation is driven by the nature of the data signals, which are, by definition, random with continually varying frequency content. As an example, for 2.5-Gb/s operation, the 3-dB bandwidth of the S_{21} response is normally specified to be greater than 2.2 GHz. The phase linearity of the S_{21} electrooptic response, describing the linear phase offset error during the electrical-to-optical conversion at a particular frequency, must be less than $\pm 5^\circ$ over the operating frequency band. The S_{11} parameter, or the electrical return loss at the modulator drive port, is also of great importance. The S_{11} value must typically be less than -10 dB, in order that the reflected power returning to the high-speed drive electronics is low and that there is <5% reduction in electrooptic conversion efficiency.

The optical extinction ratio describes the ability of the device to extinguish the light when the modulator is driven to a "zero" state. The extinction ratio is typically required to be greater than 20 dB at dc for digital applications. Variation in the modulator's electrooptic response with frequency and some small amount of reflected RF power between the modulator and driver reduce the observed extinction ratio for a PRBS signal. The optical "eye" extinction is one of the most important figures of merit for the signal, especially when cascading a number of link sections and optical amplifiers. From [41], the expression for link power penalty as a function of extinction ratio is

$$Ppen(r) \approx -10 \cdot \log\left[\frac{r-1}{r+1}\right]$$

where r is the linear ratio of ON power to OFF power. An increase in extinction ratio from 10 dB ($r = 10$) to an extinction ratio of 20 dB ($r = 100$) results in ~0.8-dB improvement in receiver sensitivity. For appropriately designed transmitters utilizing $LiNbO_3$ modulators, 20 dB extinction at frequency and >90% eye opening has been demonstrated at 2.5 Gb/s. These transmitters readily maintain >15 dB extinction under all operating conditions. At 10 Gb/s, >15 dB extinction has been achieved at frequency and >13 dB maintained over all conditions.

Modulator chirp must be taken into consideration in the link design, due to its interaction with dispersive effects. One of the major strengths of $LiNbO_3$ modulators is that they can be designed to have zero chirp and suffer no link length penalty due to dispersive interaction. However, to solve some of today's higher bit-rate problems, the ability to design a nonzero-chirp $LiNbO_3$ modulator has also proved important. The design of the modulator's chirp value is used as a degree of freedom, which can be leveraged to extend link distances. Chirp has been shown to

TABLE II
MODULATION FORMATS

Modulation Technique	Optical spectra	Data format	Comments
AM – NRZ (Amplitude Modulated – Non-Return –to-Zero)	Double sideband, with carrier	NRZ (typical)	Bandwidths typically twice the information bandwidth (or more), significant carrier power.
AM - RZ (Amplitude Modulated – Return-to-Zero)	Double sideband, with carrier	RZ	Bandwidths typically 4 times the information bandwidth (or more), significant carrier power
SSB (Single Sideband)	Single sideband	NRZ	Bandwidths ½ AM bandwidths Increased dispersion tolerance
DSSC (Double-Sideband Suppressed Carrier)	Double sideband suppressed carrier	Duo-Binary	Requires special modulation techniques, external modulator typically used
PM (Phase Modulated)	Phase modulation	PM	Used for linewidth broadening and dispersion compensation.

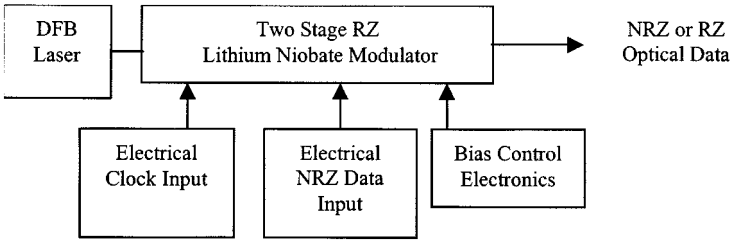

Fig. 8. Pulse-data modulator topology for RZ transmission.

enhance the transmission distances at 10 Gb/s by 25% (from 80 to 100 km) [42].

The very high DWDM channel loading (100 channels or more), the increased bit-rate requirements of next-generation systems, and the desire to build wavelength-intelligent networks has pushed the capabilities of the NRZ transmission to its limits. Hence, other data-encoding formats and modulation techniques, as described in Table II, are being considered to improve system performance. Lithium niobate affords the advantages of a customizable modulator device technology that can be used to supply enabling building blocks for these alternative modulation formats and techniques.

The return-to-zero modulation format has been employed in recent high-bandwidth terrestrial and submarine systems, especially those requiring long transmission distances. Dispersion managed soliton and other narrow-pulse transmission techniques can be considered specialized versions of RZ transmission. In conventional NRZ pulse format, the interaction between self-phase modulation (SPM) and group velocity dispersion (GVD) causes the transfer of energy from the center of the pulse toward the pulse edges [43], [44], a situation that is enhanced for a stream of "ones." Cross-phase modulation (XPM) worsens for a stream of "ones," as well, due to the increased cross-wavelength interaction time. Use of the RZ format in a dispersion-managed system greatly reduces SPM and GVD pulse deformation, resulting in greater pulse-to-pulse consistency. The improved performance permits lower optical power levels, due to the reduced duty cycle, which in itself provides additional relief from the nonlinear effects.

RZ modulation increases the demands on bandwidth and phase linearity for both the modulator and the drive electronics. Hence, modulator suppliers have designed multistage $LiNbO_3$ devices, which ease these requirements. Specifically, the bandwidth requirement for the higher spectral-width RZ format is divided into two optical stages, each with lower frequency drives. Fig. 8 shows a RZ transmitter topology implemented using a two-stage $LiNbO_3$ device. The output of such a RZ transmitter is shown in Fig. 9. NRZ input signal and RZ transmitted data at 10 Gb/s are shown in Fig. 9. These RZ transmitters have also been extended to include a third stage, which provides phase modulation, used to synchronously chirp the pulse train and extend even further the transmission link span.

The ability to integrate multiple functions into a single component has been a powerful attribute of $LiNbO_3$ modulators, driven by the desire to solve system-related challenges using the capabilities of the $LiNbO_3$ chip. Multifunction $LiNbO_3$ components can be realized with a variety of integrated-optical structures connected in series, parallel, or a combination of both.

Parallel-integration approaches are attractive in areas of the network where signals pass through multiplexers and demultiplexers. In these cases, many wavelengths, propagating in separate fibers, are present on a single card and arrayed devices (the integration of multiple-parallel channel paths on a single chip) are particularly useful. Applications such as photonic switching [45], channel-to-channel attenuation, and 3-R regeneration within line equipment are some of the drivers for parallel-integration technology.

In other applications, multiple component functions are integrated in series. For example, an integrated phase modulator and amplitude modulator can be used to provide adjustable chirp to the modulated signal launched into a network, allowing for ex-

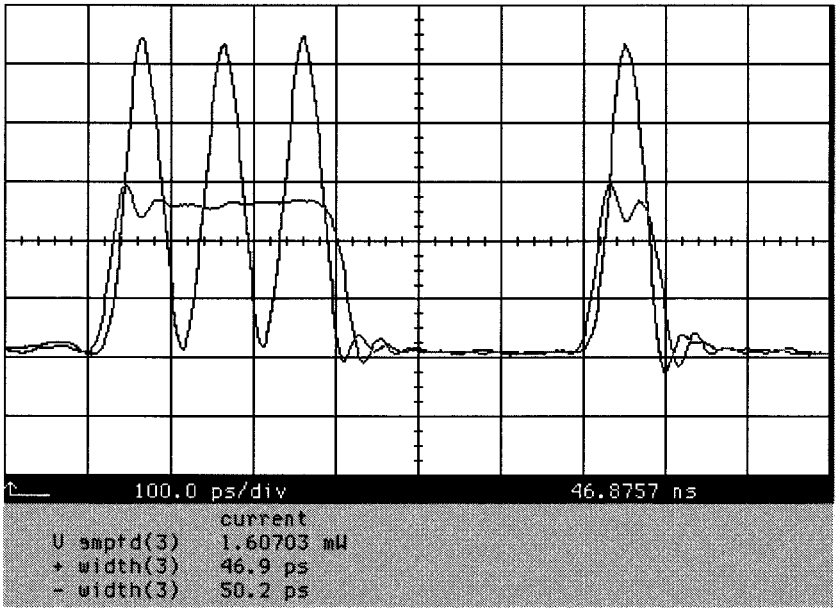

Fig. 9. Acquired waveforms of 10-Gb/s NRZ and RZ data.

tended reach in networks using dispersive fiber. Another practical example of serially combining functions is the integration of the optical data modulator with an on-chip variable attenuator. Today's DWDM systems require channel-to-channel variable attenuation for dynamic power equalization [41] and full channel blocking during live-card installations (hot swaps). Today, several $LiNbO_3$ component suppliers are integrating the attenuation and modulation functions into a single package.

Future-generation wavelength-agile networks will require modulation components to be wavelength independent and to operate in wavelength bands outside the traditional C-band of 1530–1565 nm. New systems are encompassing the L-band of 1570–1610 nm. Lithium niobate modulators have been designed to maintain low loss and constant switching voltage over the 1530–1610-nm wavelength range. As optical-amplifier technology matures, new markets will develop for modulators and other optical components at many wavelengths. Lithium niobate's broad wavelength flexibility will be invaluable in construction of these devices. As an example, future networks may use tunable lasers to provide wavelength-selectable transmission sources to add functionality, such as wavelength routing, and to help solve sparing and inventory issues [47]. Tunable laser transmitters require the use of an external modulator in order to provide a high-quality transmission signal, while maintaining wavelength-stabile operation. The modulator must have a broad-band response to wavelength in order to provide consistent performance over the entire tuning range of the laser. Laboratory demonstrations of tunable lasers, modulated with $LiNbO_3$ modulators, have been successfully performed.

V. Nondigital Applications

In the environment of the late 1990's, where WDM-based digital systems are being deployed in high volume, it is easy to overlook the equally important role of $LiNbO_3$ modulators in nondigital applications. Commercially available $LiNbO_3$ modulators are today being deployed in a variety of lower volume nondigital communications applications, such as CATV signal distribution and wide-band microwave signal distribution and antenna remoting.

It is generally accepted that high-quality, "head-end" CATV signal distribution (typically, 40–860 MHz) was the first truly successful commercial application of $LiNbO_3$ external modulator technology. State-of-the-art CATV modulators are specialized, high-performance devices. They typically include an amplitude modulator, a phase modulator for suppression of stimulated Brillouin scattering, a separate bias port, and two complementary optical outputs. The amplitude modulator must have a flat electrooptic (S_{21}) response (±0.5 dB) and low electrical return loss ($S_{11} < -18$ dB). An extensive review of external modulation for CATV signal distribution can be found in [48].

Traditionally, electronic predistortion of the CATV electrical signal has been required in order to limit the inherent nonlinear, odd-order distortion products arising from the optical modulator [49]. The development and successful commercialization of optically linearized modulators has virtually eliminated the need for such electronic predistortion and its associated finely tuned predistortion circuitry [50]. Either method can be used to transmit signals with low distortion and high carrier-to-noise ratio.

One example of an optically linearized modulator uses two independent amplitude modulators connected in series via a directional coupler. A second directional coupler is required at the output of the second amplitude modulator. The RF input (amplitude and phase) to each of the two series modulators is controlled separately. In order to achieve adequate reduction of the distortion product, the linearized modulator requires that the two directional couplers be fabricated with coupling angles within 2% (i.e., 4°) of one another. This represents a fairly tight, yet achievable, manufacturing tolerance.

The flat attenuation-versus-frequency characteristic of optical fiber makes it an ideal medium for microwave and millimeter-wave transmission, as opposed to lossy coaxial

cable or heavy metallic waveguides. For this reason, high-speed external modulators have been the object of intense research and development since the inception of $LiNbO_3$ guided-wave devices. In the last few years, packaged $LiNbO_3$ devices with bandwidths in excess of 40 GHz [51] have been demonstrated. Responses up to 100 GHz have been measured in a probed device [52].

In spite of these recent advances, the deployment of true microwave frequency links has not been widespread. They have typically been limited to military and aerospace applications where multioctave bandwidths and long-distance transmission for microwave frequencies are required [53]. These applications include radar delay lines, towed aircraft decoys and wide-band antenna remoting for distances greater than 100 m.

The widespread acceptance of multigigahertz links has been hampered by the relatively high drive voltages required by commercially available modulators, typically in the 6–10 V range at 10 GHz, and even larger at higher frequencies. Modulator drive voltages of this magnitude require signal amplification in the 35–45 dB range, assuming about 2–3 mA of detector current. Unlike digital systems whose wide-bandwidth signal is carried directly as generated, RF distribution systems have the option of down-conversion to lower frequencies, which can be transported with much lower losses on standard coaxial cables. For $LiNbO_3$ to achieve widespread deployment in wide-band, multigigahertz analog systems, a truly transparent link (0 dB electrical loss) is needed. This requires an increase in modulation efficiency by one or two orders of magnitude. A detailed treatment of intensity modulation in analog fiber-optic links may be found in [54].

VI. Product Development and Manufacturability

Like all manufactured products, the manufacturability of $LiNbO_3$ electrooptic modulators is established in the product design and development cycle. The job of the product development team is to anticipate and understand the manufacturing issues in order to generate product designs that meet high performance requirements and that can be built in volume on the production floor. The primary challenge in realizing a manufacturable design during the product-development process stems from the tradeoffs among performance, "standard" manufacturing process capability, and development time.

The importance of "time to market" in the photonic telecommunications industry cannot be underestimated. Because the industry is moving at an extremely rapid pace, product-development cycle time is as critical as performance. This is especially true for photonic components, like $LiNbO_3$ electrooptic modulators. System engineers need components that meet performance specifications, but they also need components that are available in the time frame of their system design window. In addition, the device design must be able to rapidly transition to high-volume production to meet the demands of today's fast-paced communications marketplace.

Modular designs that use standard design elements and standard manufacturing processes enable the reduction of product-development cycle times, while simultaneously ensuring manufacturability. Standard manufacturing processes used in the production of $LiNbO_3$ electrooptic modulators can

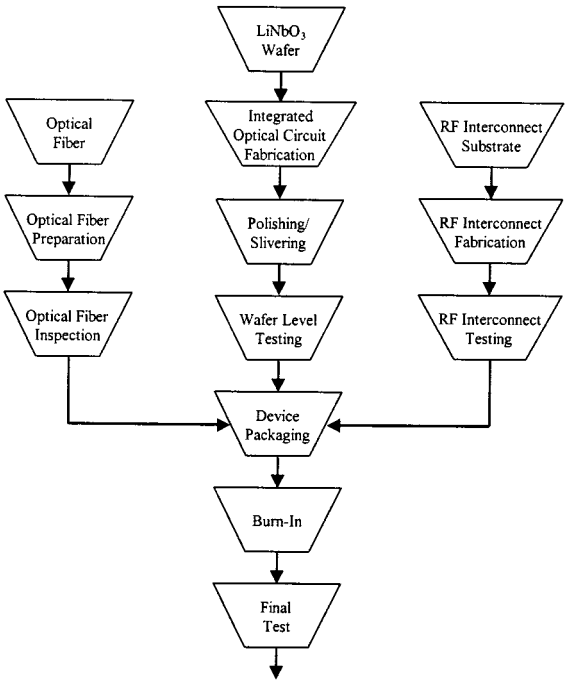

Fig. 10. The generic sequence of steps required to produce $LiNbO_3$ electrooptic modulators.

be categorized into three general groups. These are integrated optical circuit fabrication, device packaging, and testing. Each of these can be further categorized. For example, integrated optical circuit fabrication consists of waveguide processes, buffer layer processes, electrode processes, etc. Device packaging consists of RF interconnection, optical interconnection, soldering and sealing processes, etc. Testing consists of in-process testing, wafer-level testing, final device testing, etc. The generic sequence of steps required to produce $LiNbO_3$ electrooptic modulators is shown in Fig. 10.

Standardization within each process across different products, reduces performance variability, simplifies material requirements, reduces development time, and ultimately yields more manufacturable products in production. Through solid design rules and standardization of processes, $LiNbO_3$ modulator technology has rapidly transitioned from a laboratory research topic to high-volume manufacturing. Over the past five years, more than 100 000 $LiNbO_3$ modulator devices have been deployed in commercial fiber-optic communication systems.

VII. Reliability

An important device performance parameter for $LiNbO_3$ modulators is field reliability. Adequate field data are becoming available to confirm and corroborate qualification and long-term reliability predictions. The field results demonstrate that stability; performance and reliability have reached levels only speculated of a few years ago. Table III shows actual field experience for two of the more common types of $LiNbO_3$ modulators.

The calculated failure rates in Table III assume that field failures are random and are best described by an exponential distribution. The confidence intervals are calculated using a chi-

TABLE III
FIELD FAILURE RATES FOR $LiNbO_3$ MODULATORS

FIELD DATA	2.5 Gb/s, X-Cut, Ti Waveguide	2.5 Gb/s, X-Cut, APE Waveguide
In-service device hours	> 100,000,000	> 300,000,000
FIT rate at 60% confidence	9	10
FIT rate at 95% confidence	30	21

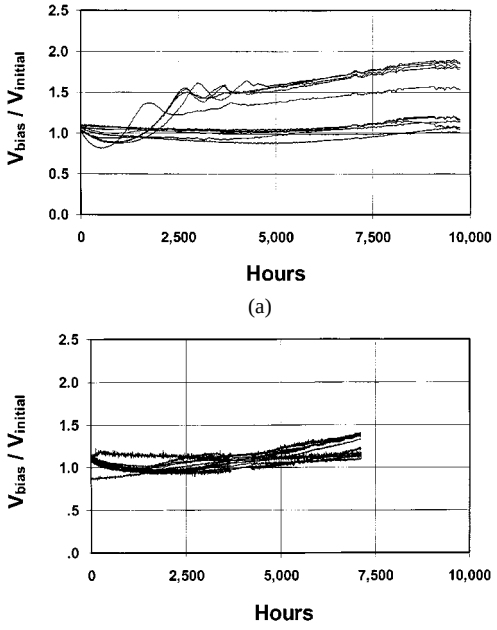

Fig. 11. Bias voltage drift for 2.5 Gb/s, x-cut, Ti modulators at (a) 85 and (b) 100 °C [19].

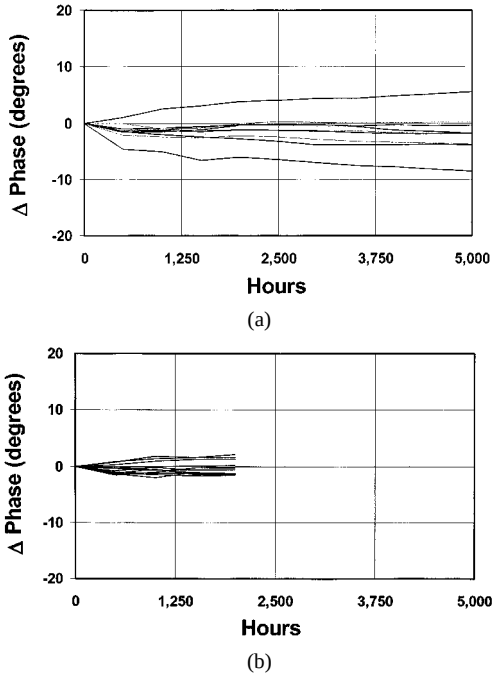

Fig. 12. Phase drift for 2.5 Gb/s bias free, x-cut, APE modulators at (a) 85 and (b) 100 °C [19].

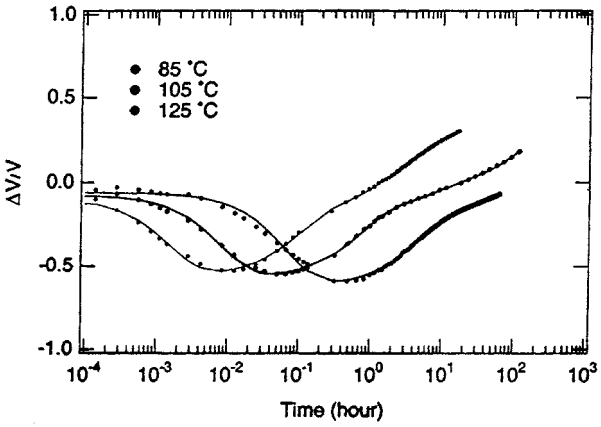

Fig. 13. Bias voltage drift at various temperatures, 10 Gb/s, z-cut, Ti modulators, from Minford [55].

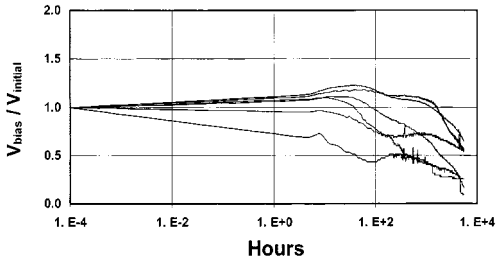

Fig. 14. Bias voltage drift at 85 °C, 10 Gb/s, x-cut, Ti waveguides [19].

squared estimator. FIT stands for failures in time per 10^9 device hours, i.e., parts per billion. As can be seen from the table, the field failure rates for the listed devices are extremely low.

One of the largest concerns during the development of $LiNbO_3$ technology was the issue of bias drift. Along with the availability of a significant amount of field data, the results from long-term accelerated aging studies are also becoming available. The results strongly suggest that bias drift is not a failure mechanism in properly designed and manufactured devices. Figs. 11–14 show the results of bias drift studies on a number of device types from different manufacturers. Clearly, all of these curves show excellent behavior.

Fig. 11(a) and (b) shows the drift of x-cut 2.5-Gb/s titanium-diffused waveguide devices at 85 and 100 °C, respectively. Both sets exhibit asymptotic limiting behavior to values below a doubling of the initial bias voltage, the general figure of merit used for the fail criteria in long-term aging studies. Fig. 12 shows the drift in bias point (measured in degrees of phase) for x-cut 2.5-Gb/s APE waveguide devices also at 85 and 100 °C. These are bias-free device designs, where the operating point at 0 V bias has been set to quadrature through specialized manufacturing processes, so bias voltage is, by definition, zero. Studies measuring the extinction ratio of pseudorandom bitstreams demonstrate that system performance is not affected by phase drifts well beyond the values seen with these bias-free designs.

Fig. 13 shows data from the literature for z-cut 10-Gb/s titanium waveguide devices at various temperatures. These data also predict adequate reliability. Fig. 14 shows the drift of x-cut 10-Gb/s titanium waveguide devices at 85 °C. The significant

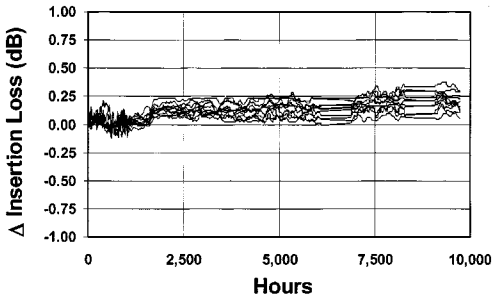

Fig. 15. Change in insertion loss with time, 85 °C, 2.5 Gb/s, x-cut, Ti modulators [19].

characteristic of Fig. 14 is the trend toward 0 V rather than the usual increasing voltage with time. This strongly suggests that drift will not be a failure mechanism. The final curve, shown in Fig. 15, is the change in insertion loss for x-cut 2.5-Gb/s titanium waveguide devices at 85 °C. As can be seen, loss changes are minimal as test time approaches 10 000 h. This loss stability is a direct indicator of the reliability of the fiber to modulator interface and a strong indicator of the optical circuit robustness.

There are many other reliability and qualification tests in addition to long-term aging studies. Telecordia (formerly Bellcore) TR-NWT-000 468 "Reliability assurance practices for optoelectronic devices in interoffice applications" [56] is the industry standard; however, it is about to be updated with GR-468-CORE "Generic reliability assurance requirements for optoelectronic devices used in telecommunications equipment" [57]. This updated version includes, for the first time, external modulators and consists of 13 different tests grouped into mechanical (mechanical shock, vibration, thermal shock, solderability, and fiber pull), endurance (accelerated aging, high temperature storage, low temperature storage, temperature cycling, damp heat, and cyclic moisture resistance), and special (internal moisture and electrostatic discharge threshold) categories. It also distinguishes between hermetic and nonhermetic components as many of the device types in commercial use are not hermetic. Although passing a particular test does not quantify reliability, it does take into account the extensive experience of Telecordia as to what is important to reduce the risk of field failure problems. The data shown in Figs. 11, 12, and 14 are from qualification programs [19] in accordance with the Telecordia requirements.

VIII. Summary

$LiNbO_3$ modulators have found widespread use in fiber-optic communication systems, including both chirped and zero-chirp NRZ and RZ digital transmission formats. In addition, these integrated-optic devices have proven to be extremely reliable, and device-manufacturing technology has progressed to enable extensive deployment within digital and analog communication systems. As the complexity of fiber-optic transmission systems and networks continues to grow, the capabilities and benefits of $LiNbO_3$ modulators should continue to develop, thereby providing new solutions and enabling new architectures.

References

[1] F. Heismann, S. K. Korotky, and J. J. Veselka, "Lithium niobate integrated optics: Selected contemporary devices and system applications," in *Optical Fiber Telecommunications III B*, I. P. Kaminow and T. L. Koch, Eds. New York: Academic, 1997, pp. 377–462.

[2] E. J. Murphy, "Photonic switching," in *Optical Fiber Telecommunications III B*, I. P. Kaminow and T. L. Koch, Eds. New York: Academic, 1997, pp. 463–501.

[3] E. J. Murphy, Ed., *Integrated Optical Circuits and Components: Design and Applications*. New York: Marcel Dekker, Aug. 1999.

[4] S. K. Korotky and R. C. Alferness, "Time and frequency domain response of directional coupler travelling wave optical modulators," *J. Lightwave Technol.*, vol. LT-1, pp. 244–251, 1983.

[5] S. K. Korotky, "Three space representations of phase mismatch switching in coupled two-state optical switching," *IEEE J. Quantum Electron.*, vol. QE-22, pp. 952–958, 1986.

[6] R. V. Schmidt and I. P. Kaminow, "Metal-diffused optical waveguides in $LiNbO_3$," *Appl. Phys. Lett.*, vol. 25, pp. 458–460, 1974.

[7] P. G. Suchoski, T. K. Findakly, and J. Leonberger, "Stable low-loss proton-exchanged $LiNbO_3$ waveguide devices with no electro-optic degradation," *Opt. Lett.*, vol. 13, pp. 1050–1052, 1988.

[8] J. L. Jackel, C. E. Rice, and J. Veselka, "Proton exchange for high-index waveguides in $LiNbO_3$," *Appl. Phys. Lett.*, vol. 41, pp. 607–608, 1982.

[9] A. Yi-Yan, "Index instabilities in proton-exchanged $LiNbO_3$ waveguides," *Appl. Phys. Lett.*, vol. 42, pp. 633–635, 1983.

[10] A. Yi-Yan, J. Primot, J. Burgeat, and R. Guglielmi, "Proton-exchanged $LiNbO_3$ waveguides: An X-ray analysis," in *Proc. 2nd ECIO*, Florence, Italy, Oct. 1983, pp. 17–18.

[11] R. A. Becker, "Comparison of guided-wave interferometric modulators fabricated on $LiNbO_3$ via Ti indiffusion and proton exchange," *Appl. Phys. Lett.*, vol. 43, pp. 131–133, 1983.

[12] K. M. Kissa, P. G. Suchoski, and D. K. Lewis, "Accelerated aging of annealed proton-exchanged waveguides," *J. Lightwave Technol.*, vol. 13, pp. 1521–1529, 1995.

[13] D. K. Lewis, K. M. Kissa, and P. G. Suchoski, "Long lifetime projections for annealed proton-exchanged waveguide devices," *IEEE Photon. Technol. Lett.*, vol. 7, pp. 1318–1320, 1995.

[14] K. Noguchi, O. Mitomi, H. Miyazawa, and S. Seki, "A broadband $Ti:LiNbO_3$ optical modulator with a ridge structure," *J. Lightwave Technol.*, vol. 13, pp. 1164–1168, 1995.

[15] F. Laurell, J. Webjorn, G. Arvidsson, and J. Holmberg, "Wet etching of proton-exchanged lithium niobate - A novel processing technique," *J. Lightwave Technol.*, vol. 10, pp. 1606–1609, 1992.

[16] W. L. Chen, R. S. Chen, J. H. Lee, and W. S. Wang, "Lithium niobate ridge waveguides by nickel diffusion and proton-exchanged wet etching," *IEEE Photon. Technol. Lett.*, vol. 7, pp. 1318–1320, 1995.

[17] K. Noguchi, O. Mitomi, K. Kawano, and M. Yanagibashi, "Highly efficient 40-GHz bandwidth $Ti:LiNbO_3$ optical modulator employing ridge structure," *IEEE Photon. Technol. Lett.*, vol. 5, pp. 52–54, 1993.

[18] R. S. Moyer, R. Grencavich, F. F. Judd, R. C. Kershner, W. J. Minford, and R. W. Smith, "Design and qualification of hermetically packaged lithium niobate optical modulator," *IEEE Trans. Comp., Packag., Manufact. Technol. B*, vol. 21, pp. 130– 135, 1998.

[19] D. Maack , "Reliability of lithium niobate Mach- Zehnder modulators for digital optical fiber telecommunication systems," in *Proc. SPIE Critical Reviews: Reliability of Optical Fibers and Optical Fiber Systems*, Boston, MA, Sept. 1999, pp. 197–230.

[20] A. O'Donnell, "Packaging and reliability of active optical components," in *Proc. 7th Eur. Conf. Int. Opt. (ECIO '95)*, 1995, p. 585.

[21] R. C. Alferness, "Waveguide electro-optic modulators," *IEEE Trans. Microwave Theory Tech.*, vol. MTT-30, pp. 1121–1137, Aug. 1982.

[22] R. V. Schmidt and R. C. Alferness, "Directional coupler switches, modulators, and filters using alternating techniques," *IEEE Trans. Circuits Syst.*, vol. CAS-26, pp. 1099–1108, 1979.

[23] Y. Silberberg, P. Perlmutter, and J. E. Baran, "Digital optical switch," *Appl. Phys. Lett.*, vol. 51, pp. 1230–1232, 1987.

[24] W. K. Burns, A. B. Lee, and A. F. Milton, "Active branching waveguide modulator," *Appl. Phys. Lett.*, vol. 29, pp. 790–792, 1976.

[25] W. K. Burns, "Shaping the digital switch," *IEEE Photon. Technol. Lett.*, vol. 4, pp. 861–863, 1992.

[26] H. Okayama and M. Kawahara, "Prototype 32x32 optical switch matrix," *Electron. Lett.*, vol. 30, pp. 1128–1129, 1994.

[27] T. O. Murphy, E. J. Murphy, and R. W. Irvin, "An 8 x 8 Ti : LiNbO3 polarization independent photonic switch," in *Proc. Photonics in Switching/ECOC*, Florence, Italy, 1994 , pp. 174–176.

[28] K. Noguchi, O. Mitomi, and H. Miyazawa, "Millimeter-wave Ti : $LiNbO_3$ optical modulators," *J. Lightwave Technol.*, vol. 16, pp. 615–619, 1998.
[29] H. A. Wheeler, "Formulas for the skin effect," *Proc. IRE*, vol. 30, pp. 412–424, 1942.
[30] S.-J. Chang, C.-L. Tsai, Y.-B. Lin, J.-F. Liu, and W.-S. Wang, "Improved electro-optic modulator with ridge structure in x-cut $LiNbO_3$," *J. Lightwave Technol.*, vol. 17, pp. 843–847, 1999.
[31] D. W. Dolfi and T. R. Ranganath, "50 GHz velocity-matched, broad wavelength $LiNbO_3$ modulator with multimode active section," in *Proc. Integrated Photonics Research Conf.*, 1992, post-deadline paper PD-2.
[32] R. C. Alferness, S. K. Korotky, and E. A. J. Marcatilli, "Velocity matching techniques for integrated optic traveling wave switch/modulators," *J. Lightwave Technol.*, vol. 20, pp. 301–309, 1984.
[33] P. Hallemeier, K. Kissa, G. McBrien, and T. Horton , "Next generation 10Gb/s lithium niobate modulator components for RZ based transmission techniques," in *Proc. National Fiberoptic Engineers Conf.*, Sept. 1999.
[34] K. Imai, T. Tsuritani, N. Takeda, K. Tanaka, N. Edagawa, and M. Suzui, "500 Gb/s (50x10 Gb/s) WDM transmission over 4000km using broadband EDFA's and low dispersion slope fiber," in *Tech. Dig. Optical Fiber Communication Conf.*, Feb. 1999, post-deadline paper PD5.
[35] G. Gopalakrishnan, W. K. Burns, R. W. McElhanon, C. H. Bulmer, and A. S. Greenblatt, "Performance and modeling of broadband $LiNbO_3$ traveling wave optical intensity modulators," *J. Lightwave Technol.*, vol. 12, pp. 1807–1819, 1994.
[36] S. K. Korotky and J. J. Veselka, "An RC network analysis of long term Ti :$LiNbO_3$ bias stability," *J. Lightwave Technol.*, vol. 14, pp. 2687–2697, 1996.
[37] N. S. Bergano, C. R. Davidson, C. J. Chen, B. Pederson, M. A. Mills, N. Ramanujam, H. D. Kidorf, A. B. Puc, M. D. Levonas, and H. Abdelkader, "640 Gb/s transmission of sixty-four 10 Gb/s WDM channels over 7200km with 0.33 (bits/s)/Hz spectral efficiency," in *Tech. Dig. Optical Fiber Communication Conf.*, Feb. 1999, post-deadline paper PD2.
[38] W. K. Burns, "Linearized optical modulator with fifth order correction," *J. Lightwave Technol.*, vol. 13, pp. 1724–1727, 1995.
[39] G. E. Betts, "Microwave analog optical links using suboctave linearized modulators," *IEEE Photon. Technol. Lett.*, vol. 8, pp. 1273–1275, 1996.
[40] M. Izutsu, S. Shikama, and T. Sueta, "Integrated optical SSB modulator/frequency shifter," *IEEE J. Quantum Electron.*, vol. QE-17, pp. 2225–2227, 1981.
[41] R. Ramaswami and K. Sivarajan, *Optical Networks: A Practical Perspective*. Los Altos, CA: Morgan Kaufmann, 1998.
[42] G. P. Agrawal, *Non-Linear Fiber Optics*, 2nd ed. New York: Academic, 1995.
[43] F. M. Madani and K. Kikuchi, "Design of long-distance WDM dispersion managed transmission system," *J. Lightwave Technol.*, vol. 17, pp. 1326–1335, 1999.
[44] M. I. Hayee and A. E. Wilner, "NRZ versus RZ in 10-40 Gb/s dispersion-managed WDM transmission systems," *IEEE Photon. Technol. Lett.*, vol. 11, pp. 991–993, 1999.
[45] E. J. Murphy, "Photonic switching," in *Optical Fiber Telecommunications IIIB*, I. P. Kaminow and T. L. Koch, Eds. New York: Academic, 1997, ch. 10, pp. 463–501.
[46] M. G. Taylor and S. J. Penticost, "Improvement in performance of long haul EDFA using high frequency polarization modulation," *Electron. Lett.*, vol. 30, no. 10, pp. 805–806, 1994.
[47] R. Plastow, "Tunable lasers enable new optical networks to meet changing demands," *Lightwave*, pp. 74–79, Dec. 1998.
[48] W. Way, *Broadband Hybrid Fiber/Coax Access System Technologies*. New York: Academic, 1999, ch. 7.
[49] G. Wilson, "Predistortion techniques for linearization of external modulators," in *Dig. IEEE/LEOS Summer Topical Meeting*, San Diego, CA, July 26–30, 1999, paper FB2.1., pp. 26–30.
[50] H. Skeie, "An optically linearized modulator for CATV applications," in *Proc. SPIE*, vol. 2291, 1994, pp. 227–238.
[51] W. Burns, M. Howerton, R. Moeller, R. McElhanon, and S. Greenblatt, "Low drive voltage, 40 GHz $LiNbO_3$ modulators," in *OFC '99*, San Diego, CA, Feb. 1999, paper ThT1.
[52] K. Noguchi, O. Mitomi, and H. Miyazawa, "Low voltage and broadband Ti : $LiNbO_3$ optical modulator operating in the millimeter wavelength region," in *Tech. Dig. Conf. Optical Fiber Communications*, San Francisco, CA, Jan. 1996, paper ThB2, pp. 205–206.
[53] D. Lafaw, R. Logan, and F. Leonberger, "Multi-GHz components: An industrial perspective," presented at the International Topical Meeting on Microwave Photonics, MWP '99, Melbourne, Australia, Nov. 1999.
[54] C. Cox, E. Ackerman, R. Helkey, and G. Betts, "Techniques and performance of intensity-modulation direct-detection analog optical links," *IEEE Trans. Microwave Theory Tech.*, vol. 45, pp. 1375–1383, Aug. 1997.
[55] W. Minford, "The taming of $LiNbO_3$," in *FIO III*, St. Martin Vesubie, France, slide presentation.
[56] "Reliability assurance practices for optoelectronic devices in interoffice applications," Bellcore, TR-NWT-000 468, Dec. 1991.
[57] "Generic reliability assurance requirements for optoelectronic devices used in telecommunications equipment," Bellcore, GR-468-CORE, Dec. 1998.

Ed L. Wooten (M'92) received the B.S. degree in electrical engineering from the Massachusetts Institute of Technology, Cambridge, in 1982 and the M.S. and Ph.D. degrees in applied physics from the University of California at San Diego, La Jolla, CA, in 1991.

His graduate work concerned the modeling and fabrication of guided wave electrooptic modulators in lithium niobate. From 1993 to 1997, he worked at Tetra Tech Data Systems, Carlsbad, CA, on the development of a rapidly tunable wavelength filter, fused fiber optic couplers, and a secure optical homodyne communication system. In 1997, he joined the staff at JDS Uniphase, where he is responsible for the design of custom $LiNbO_3$ modulators and new product development.

Karl M. Kissa (S'86–M'88) received the B.S. degree from Duke University, Durham, NC, in 1982 and the Ph.D. degree from University of Delaware, Newark, in 1989.

From 1989 to 1994, he was a Member of Technical Staff at Charles Stark Draper Laboratory, Cambridge, MA, where he designed integrated optical (IO) lithium niobate devices for fiber-optic gyroscopes. In 1994, he joined JDS Uniphase, where he models and designs lithium niobate devices. He was also involved in the development of acousto-optic tunable filters.

Alfredo Yi-Yan received the B.Sc. and Ph.D. degrees in electronics and electrical engineering from the University of Glasgow, Scotland, U.K., in 1974 and 1978, respectively.

From 1978 to 1981, he was a SERC Research Assistant at the Electronics and Electrical Engineering Department, University of Glasgow, working on periodic waveguide filters for integrated optics. In 1981, he joined CNET-Laboratoire de Bagneux, Paris, France, and was engaged in work on lithium niobate devices, as well as active and passive periodic waveguides in semiconductors. In 1987, he left CNET to join Bellcore as a Member of Technical Staff, a position that he held until 1992. At Bellcore, his research interest focused on advanced optical components for fiber-optics communications systems and hybrid integration techniques. He has been with JDS Uniphase since 1997, where he is currently engaged in process-development activities.

Edmond J. Murphy (SM'94) received the B.S. degree in chemistry from Boston College, Boston, MA, in 1976 and the Ph.D. degree in chemical physics from Massachusetts Institute of Technology, Cambridge, in 1980.

From 1980 to 1999, he was a Distinguished Member of Technical Staff and Technical Manager at Lucent Technologies. At Lucent, he was involved with work on optical amplifiers, lithium niobate devices, and optical data links. He is currently Director of Technology for JDS Uniphase's Electro-optic Product Division in Bloomfield, CT. He holds 12 patents and is the author of more than 50 technical publications.

Dr. Murphy is a Fellow of the Optical Society.

Donald A. Lafaw received the B.S. degree (with high honors) and the M.S. degree in electrical engineering from the University of Illinois, Urbana, in 1983 and 1984, respectively.

From 1984 until 1997, he held various technical staff positions at the Rome Laboratory Air Force Photonics Center, Lawrence Livermore National Laboratory, National Security Agency, and the Laboratory for Physical Sciences at the University of Maryland, College Park. He is currently a Business-Unit Manager for Advanced Digital and RF Products at JDS Uniphase in Bloomfield, CT.

Peter F. Hallemeier (S'93–M'97) received the B.S.E.E. degree from Northeastern University, Boston, MA, and the M.S.E.E. degree from the University of Rochester, Rochester, NY, with concentrations in electromagnetics, RF engineering, and optoelectronics.

His research and design work has included high-temperature superconductor devices, liquid crystal devices, lithium niobate devices, and fiber systems. In 1998, he joined JDS Uniphase in Bloomfield, CT and is currently a Business Unit Manager.

David Maack (M'97) received the B.S. degree in physics and in nuclear science from Lowell Technological Institute, Lowell, MA, in 1969 and the M.B.A. degree from the University of New Haven, New Haven, CT, in 1983.

His career in fiber optics spans 25 years. He has held various developmental, engineering, manufacturing, and management positions. He is currently Manager of Reliability Engineering at JDS Uniphase in Bloomfield, CT. His current interests include failure analysis and reliability predictions for optical components.

Daniel V. Attanasio received the B.S. degree in physics from the State University of New York at Albany in 1989 and the M.S. degree from the Institute of Optics at the University of Rochester, Rochester, NY, in 1991.

He was an Optical Engineer with 3M Corp. from 1990 to 1997, performing research on $LiNbO_3$ polarization-independent integrated-optical switches and polarization-maintaining fiber-optic connectors. In 1997, he joined JDS Uniphase in Bloomfield, CT, where he is currently a Product Development Project Leader.

Daniel J. Fritz received the B.S. degree in physics from the University of Hartford, West Hartford, CT.

From 1982 to 1995, he was a Member of Technical Staff at United Technologies Research Center in East Hartford, CT. Since 1995, he has been employed at JDS Uniphase in Bloomfield, CT, and is currently a Business Unit Manager for 2.5-Gb/s lithium niobate modulators.

Gregory J. McBrien (M'94) received the B.S.E.E. and M.S.E.E. degrees from Rensselaer Polytechnic Institute, Troy, NY, in 1979 and 1997, respectively.

He joined the advanced guidance and control electronics group at Hamilton Standard Division of United Technologies Corp. from 1979 to 1990, where he worked on a number of fiber-optic sensor and data applications. He joined the United Technologies Research Center in 1990, as part of the Photonics Initiative Group, and continued with what is now JDS Uniphase, working on a number of analog and digital development products involving lithium niobate. He has 13 patents in the areas of sensors, signal processing, and fiber-optic analog and digital technology areas.

Donald E. Bossi (S'87–M'90) received the S.B., S.M., and Ph.D. degrees from the Massachusetts Institute of Technology, Cambridge, MA, in 1985, 1986, and 1990, respectively, all in electrical engineering.

From 1990 to 1993, he worked at United Technologies Research Center in East Hartford, CT, on the development of GaAs integrated optoelectronic circuits. In 1994, he joined JDS Uniphase in Bloomfield, CT, where he is presently a Vice President of Technology and Development.